Received: 14 May 2022 | Revised: 24 October 2022 | Accepted: 26 October 2022

DOI: 10.1002/mgg3.2095

Molecular Genetics & Genomic Medicine Open Access WILEY

ORIGINAL ARTICLE

BEST1 novel mutation causes Bestrophinopathies in six families with distinct phenotypic diversity

Shangying Yang[1] | **Zhen Li**[2] | **Wanyu Cheng**[1] | **Meijiao Ma**[3] | **Rui Qi**[4] | **Xue Rui**[3] | **Yinghua Ren**[2] | **Xunlun Sheng**[3] | **Weining Rong**[2]

[1]Clinical Medical College, Ningxia Medical University, Yinchuan, China

[2]Ningxia Eye Hospital, People's Hospital of Ningxia Hui Autonomous Region, Third Clinical Medical College of Ningxia Medical University, Yinchuan, China

[3]Gansu Aier Ophthalmiology and Optometry Hospital, Lanzhou City, China

[4]Aier Eye Hospital Group, Hubin Aier Eye Hospital, Binzhou City, China

Correspondence
Xunlun Sheng, Gansu Aier Ophthalmiology and Optometry Hospital, 1228-437, Guazhou Road, Qilihe District, Lanzhou City, Gansu, 730050, China.
Email: shengxunlun@163.com

Weining Rong, Ningxia Eye Hospital, People's Hospital of Ningxia Hui Autonomous Region, Third Clinical Medical College of Ningxia Medical University, No. 936, Huang He East Road, Jinfeng District, Yinchuan, 750001, China.
Email: rongweining426@126.com

Funding information
The key research and development project of Ningxi Hui Autonomous Region, Grant/Award Number: 2020BEG03047; National Natural Science Foundation of China, Grant/Award Number: 81760180; The Key R & D Plan Project of Ningxia Hui Autonomous Region, Grant/Award Number: 2021BEG02045; Ningxia Natural Science Foundation Project,

Abstract

Purpose: To report novel *BEST1* variants in six Chinese families with bestrophinopathies of two different inheritance modes and analyze the intrafamilial phenotypic diversity.

Method: A total of 25 participants including 13 patients and 12 healthy family members from 6 Chinese families with bestrophinopathies were available for genetic and clinical analysis. All of the patients were subjected to comprehensive ophthalmic evaluations and exome sequencing was performed on the probands to detect the causative variants. The pathogenicity of gene variants was predicted using silico analysis and evaluated according to ACMG guidelines. All (likely) pathogenic variants were determined by Sanger sequencing and co-segregation analyses were performed on available family members. The relevant original literature previously reported was retrieved to explore the relationship between *BEST1*-related gene variants and clinical features.

Results: In the 6 families, 3 families (10 patients) were assigned as autosomal dominant bestrophinopathies (VMD) and 3 families (3 patients) were assigned as Autosomal recessive Bestrophinopathies (ARB). A total of 9 variants on the *BEST1* gene were identified, containing 7 missense variants, 1 nonsense variant, and 1 frameshift variant, respectively, of which 3 variants c.88A > G (p.Lys30Glu), c.764G > A (p.Arg255Gln) and c.233dupT (p.Ser79Phefs*153) were novel variants. Three families with ARB were detected with heterozygous variants on the *BEST1* gene.2 families (8 patients) with BVMD showed markedly irregular dominant inheritance, and the severity of macular lesions varies greatly among individuals of the same family. Among them, the probands showed typical vitelliform lesions in the macula, while the other six patients had no visible signs of the disease by fundus photography (ophthalmoscopy) and minor lesions could be detected on OCT in two patients, the continuity of the ellipsoidal band was interrupted with the chimeric band. The phenotypes of the patients in the three ARB families ranged from typical/atypical vitelliform lesions to extensive extramacular deposits (peripheral spots).

Grant/Award Number: 2021AAC03302; The Training Project of the Scientific Innovation Commanding Talented Person in Ningxia Hui Autonomous Region, Grant/Award Number: KJT2020013

Conclusion: This study provided evidence that the phenotype of BVMD manifested irregular dominant inheritance, with patients carrying a pathogenic heterozygous variant of *BEST1* to develop obvious intrafamilial phenotypic diversity, and the patients who harbor two pathogenic alleles showed recessive inheritance bestrophinopathies with distinct phenotypic diversity. Our study also emphasized the importance of comprehensive genetic analysis in patients with bestrophinopathies, and in such challenging families with distinct intrafamilial phenotypic diversity, it shall provide novel insights into phenotypic assessments of bestrophinopathies, and contribute to better diagnosis, prognosis, and treatment for these patients.

KEYWORDS

autosomal recessive bestrophinopathies, best vitelliform macular dystrophy, *BEST1* gene, genotype and phenotype, irregular dominant inheritance

1 | INTRODUCTION

Bestrophinopathies are a group of inherited macular dystrophy disorders caused by variants in the *BEST1* gene (Marmorstein et al., 2018), among which, Best vitelliform macular dystrophy (BVMD, OMIM153700) is the first and the most commonly diagnosed *BEST1*-related retinopathy (Jay, 2012). Variants in the *BEST1* gene were later found to also cause autosomal dominant vitreoretinochoroidopathy (ADVIRC, OMIM193220) and autosomal recessive bestrophinopathies (ARB, OMIM611809). The main pathological mechanism of all three diseases is that the primary lesion is located in the retinal pigment epithelium (RPE), which in turn affects photoreceptor cells (Jay, 2012). Therefore, such three diseases are collectively referred to as "Bestrophinopathies." Variants in the *BEST1*gene potentially affect the development of the entire eyeball in addition to causing retinal lesions(Vincent et al., 2011).

The *BEST1* gene (OMIM 607854, formerly known as VMD2 gene) is located at 11q12.3, approximately 980 kb, and contains 13 exons and encodes a transchannel transporter protein consisting of 585 amino acids. It is mainly expressed in the RPE cell membrane and the kidney, brain, and colon (Johnson et al., 2017; Soria et al., 2009). The *BEST1* gene encodes the Bestrophin−1 protein localized on the basolateral membrane of RPE cells, which forms calcium-activated chloride channels and is associated with the regulation of voltage-dependent calcium channels (Wood et al., 2019). In addition, such protein is associated with eye development. When the *BEST1* gene is mutated, the Bestrophin−1 protein becomes dysfunctional, which can lead to a range of clinical manifestations. To date, 410 different variants in the *BEST1* gene have been identified, which also result in numerous phenotypes (Clinvar database).

The BVMD phenotype includes a typical yellow yolk-like macular lesion and multiple lesions and lesions outside the macula occur in at least one-quarter of affected individuals, classified into the following five clinical stages: previtelliform, vitelliform, vitelliruptive, pseudohypopion, atrophy, and cicatricial (Tsang Stephen & Tarun, 2018), but it is important to note that the disease does not progress through each of these stages in every individual. The age of onset of BVMD is mostly 3–15 years old (i.e., juvenile vitelliform dystrophy), and the onset of adult-onset vitelliform macular dystrophy (AVMD, OMIM 153700 or adult-onset foveomacular vitelliform dystrophy, AFVD) after the age of 40 years is considered a specific phenotype of BVMD and is also consistent with an autosomal dominant mode of inheritance with the similar fundus manifestations and staging as BVMD (Chowers et al., 2015). ARB is characterized by macular degeneration with extramacular scattered punctate deposits and intraretinal and subretinal fluid (SRF) accumulation. Additionally, the phenotype encompasses hyperopia, short axial-length, shallow anterior chamber, and angle closure glaucoma that can co-occur (Johnson et al., 2017). For both BVMD and ARB, the Arden ratio, especially the light peak value of the electrooculogram was significantly decreased (Johnson et al., 2017).

Bestrophinopathies have a significant clinical heterogeneity with diverse clinical presentations. The phenotype of BVMD is incompletely penetrant with some patients who carry an autosomal dominant variant in *BEST1* show no visible signs of the disease even after the age of 50 years (Mullins et al., 2005). The phenotype of ARB in some patients who carry an autosomal recessive variant in *BEST1* displays macular changes resembling the vitelliruptive, atrophic, and cicatricial stages of VMD, central serous chorioretinopathy (CSC) and advanced

stages of ADVIRC (Johnson et al., 2017). The significant clinical heterogeneity associated with *BEST1* variants highlights the need for an extensive genetic analysis and comprehensive clinical characterization of patients to better understand genotype–phenotype correlations and make an accurate diagnosis. In the present study, it is intended to identify the variants in 6 Chinese families with Bestrophinopathies, analyze the genotype and phenotype, and reveal the intrafamilial phenotypic diversity of irregular dominant inheritance.

2 | OBJECTS AND METHODS

2.1 | Clinical data collection

The relevant ophthalmologic examinations of the probands and their family members were completed, including best-corrected visual acuity (BCVA), slit-lamp microscopy, chromoptometry (5th edition color vision examination plates, Ziping YU), ocular axial length, dilated fundus examination with photography (TRC- 50DX, Topcon Inc.), optical coherence tomography (OCT, HD-OCT4000, Carl Zeiss Meditec, USA), optical coherence tomography angiography (OCTA), infrared ray (IR), electroretinogram (ERG), electrooculogram (EOG), fundus autofluorescence (FAF), and fluorescein angiography (FFA). The study was approved by the Ethical Medical Committee of Ningxia Hui Autonomous Region People's Hospital (Approval No. 2016018). All genetic testing and diagnostic works were performed subject to the consent of patients and their families by signing the informed consent forms.

2.2 | Exome sequencing

To reveal the disease-causing variant, exome sequencing was selectively performed on both the probands and their parents. Exome was captured by Agilent SureSelect exon capture kit. Sequencing was served with a high-throughput sequencer (Illumina, HiSeq Xten). The raw sequencing data were processed by Illumina basecalling Software 1.7 analysis software and subsequently compared with the NCBI human genomic DNA reference sequence (NCBI build 37.1) and analyzed by SOAP software (http://soap.genomics.org.cn) to obtain single-nucleotide variation (SNV) related information. The BWA software (http://bio-bwa.sourceforge.net/) was used to analyze the data of inserts and deletions (Indel) to acquire all the variations that occurred in the DNA sequences of the samples. After stepwise filtering, the number of variants shared by all patients in the family was screened out, and then variants unavailable with the diseased relatives in the family were filtered to obtain the candidate pathogenic variants. Sanger validation was used to exclude false positives for candidate pathogenic variants, while the presence of co-segregation was verified in normal family members.

2.3 | In silico analysis

The target variant loci were queried using database tools such as HGMD (human gene mutation database) and dbSNP (https://www.ncbi.nlm.nih.gov/snp/) to see if they were reported pathogenic variants in HGMD and to see if they had been included. Minimum allele frequency less than 0.005 as the criteria to exclude benign variants by reference to the databases for East Asian populations Allele frequencies available with Genome Aggregation Database (gnomAD, http://gnomad.broadinstitute.org/) and Exome Aggregation Consortium (ExAC, http://exac.broadinstitute.org/). Publicly available servers for bioinformatic prediction tools, such as Polyphen2 (http://genetics.bwh.harvard.edu/pph2), SIFT (http://sift.jcvi.org), PROVEAN (http://provean.jcvi.org/index.php), and Variants were classified as clinically unclear when at least 1 of 4 predictions had a benign outcome or when there was insufficient evidence of pathogenicity. When all predictions were pathogenic, variants were classified as possibly pathogenic in combination with other evidence. Frameshift variants, nonsense variants, and variants with experimental evidence of loss of protein function were classified as pathogenic variants.

Finally, the pathogenicity of the variants was assessed according to the standards and guidelines published in 2015 by the American College of Medical Genetics and Genomics (ACMG) (Richards et al., 2015).

3 | RESULTS

3.1 | Clinical phenotypes and exome sequencing results

3.1.1 | Family 1

The proband, female, 29 years old, complained of blurred vision in the left eye for 5 days. She denied any inherited disease of family history. She had a normal color vision and BCVA of 0.8 in the right eye, and 0.5 in the left eye. The anterior segment was normal, and a typical appearance of egg-yolk-like macular changes in both eyes (Figure 1). The light peak amplitude of EOG decreased significantly (Table 2) and full-field ERG was normal. The other four patients in the family had no visible signs of the disease

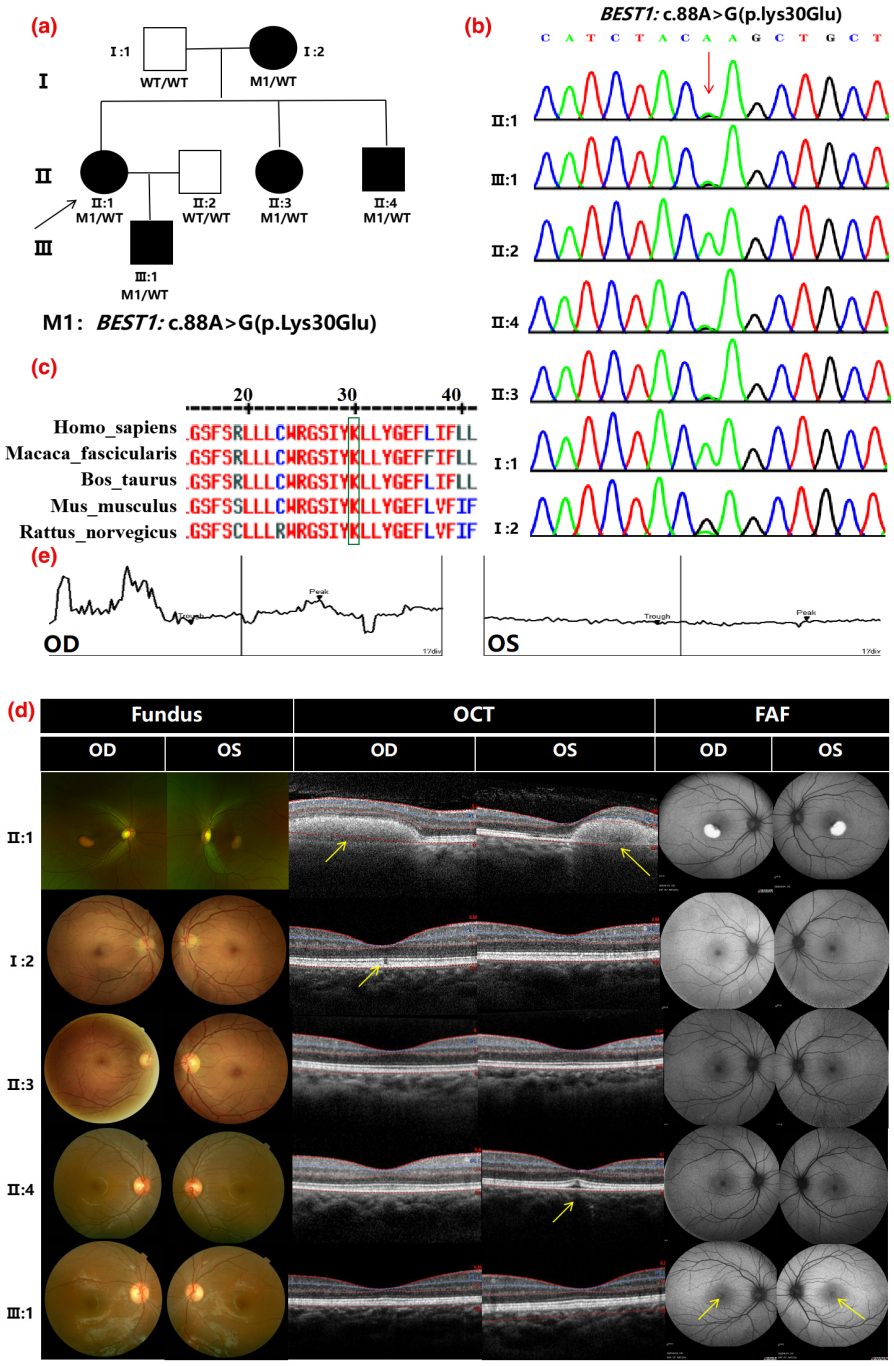

FIGURE 1 The pedigree, sequence analysis, and fundus examination of family 1 with BVMD. (a) Pedigree of family 1; (b) Sequence chromatograms of identified mutations; (c) The homology of amino acid sequences between human *BEST1* and other species. The amino acid at position 30 is highly conserved among species. The mutated residue 30 is boxed and indicated; (d) Fundus photograph: The proband (II:1) had a well-defined ovoid lesion with a size of about 1 DD and a typical appearance of egg-yolk-like changes in the macula of both eyes and no obvious abnormal changes were found in the macula of the other patients; OCT: The proband (II:1) showed the macular fovea of both eyes was raised, the ellipsoid zone and chimeric zone were raised in varying degrees, hyperreflective masses were visible below the chimeric zone, the RPE was discontinuous and partially defective. The continuity of the ellipsoid zone and chimeric zone in the right eye of the proband's mother (I:2) was interrupted, and the left eye was normal. The proband's younger brother (II:4) had an arched bulge of the ellipsoid zone and chimeric zone in the left eye, and the right eye was normal. The structures of macular areas in both eyes of the proband's son (III:1) and the proband's sister (II:3) were normal, and the structures of each layer were complete and continuous; FAF: The egg yolk-like substance in the macular area of the proband (II:1) showed high fluorescence. The son of the proband (III:1) had dot high fluorescence in the macular fovea of the right eye and ring high fluorescence in the macular fovea of the left eye. (e) The proband's EOG: the waveforms of dark valleys and light peaks are shown from left to right

TABLE 1 Clinical phenotypes of three families with autosomal dominant Bestrophinopathies

		Best-corrected visual acuity		Axial length (mm)		Anterior chamber depth (mm)					
	Object	OD	OS	OD	OS	OD	OS	Fundus	FAF	FFA	EOG
F1 patient	II:1 (29 y)	-0.50 DS/−0.50 DC ×110* = 0.8	-0.25 DS/−0.75 DC ×65* = 0.5	22.42	22.32	3.03	2.94	Vite	Hyper	Fluorescence masking at lesion, no fluorescent leakage in the late stage	abnormal
	I:2 (51 y)	+1.25 DC ×5* = 0.8	PL = 0.8	22.65	22.73	2.73	2.66	Pre	normal	normal	abnormal
	II:3 (28 y)	PL = 1.0	PL = 1.0	22.70	22.71	3.03	3.01	Pre	normal	normal	abnormal
	II:4 (25 y)	PL = 1.0	-0.50 DC ×85* = 1.0	23.57	23.44	3.46	3.44	Pre	normal	normal	NA
	III:1 (7 y)	PL = 0.8	PL = 0.6	22.60	22.64	3.39	3.26	Pre	dot/ring Hyper	normal	abnormal
F1 normal	II:2 (32 y)	-1.50 DS/−0.50 DC ×30* = 1.0	-1.25 DS = 1.0	23.79	23.76	3.32	3.34	normal	NA	NA	normal
F2 patient	I:1 (67 y)	PL = 0.15	-0.50 DS/+1.25 DC ×80* = 0.5	22.41	22.66	3.27	3.22	Vitelliruptive	flake Hypo	Dot/ring Hyper	abnormal
	II:1 (41 y)	−5.75 DS/−0.75 DC ×5* = 0.8	−6.50 DS = 1.0	24.87	24.71	3.52	3.50	Pre	normal	normal	abnormal
	III:1 (12 y)	−1.00 DS/−0.75 DC ×60* = 1.0	−1.00 DS = 1.0	23.62	23.89	3.88	3.97	Pre	normal	normal	abnormal
F2 normal	II:2 (43 y)	PL = 1.0	−0.25 DS = 1.0	NA	NA	NA	NA	normal	NA	NA	NA
F3 patient	II:2 (16 y)	−1.50 DC ×5* = 0.5	−0.25 DS/−0.75 DC ×175* = 1.0	24.22	24.02	3.22	3.32	atrophy	Hypo and hyper around	Round and flake fluorescence, with obvious late leakage	abnormal
	I:2 (45 y)	−0.50 DS/−0.50 DC ×100° = 0.6	PL = 1.0	23.02	22.94	3.36	3.35	Vite	Hyper	NA	abnormal
F3 normal	I:1 (46 y)	PL = 1.0	PL = 1.0	NA	NA	NA	NA	normal	NA	NA	NA

Abbreviations: EOG, electrooculogram; FAF, fundus autofluorescence; FFA, fluorescein angiography; Hyper, hyperfluorescence; Hypo, hypofluorescence; NA, not available; Pre, previtelliform; vite, vitelliform.

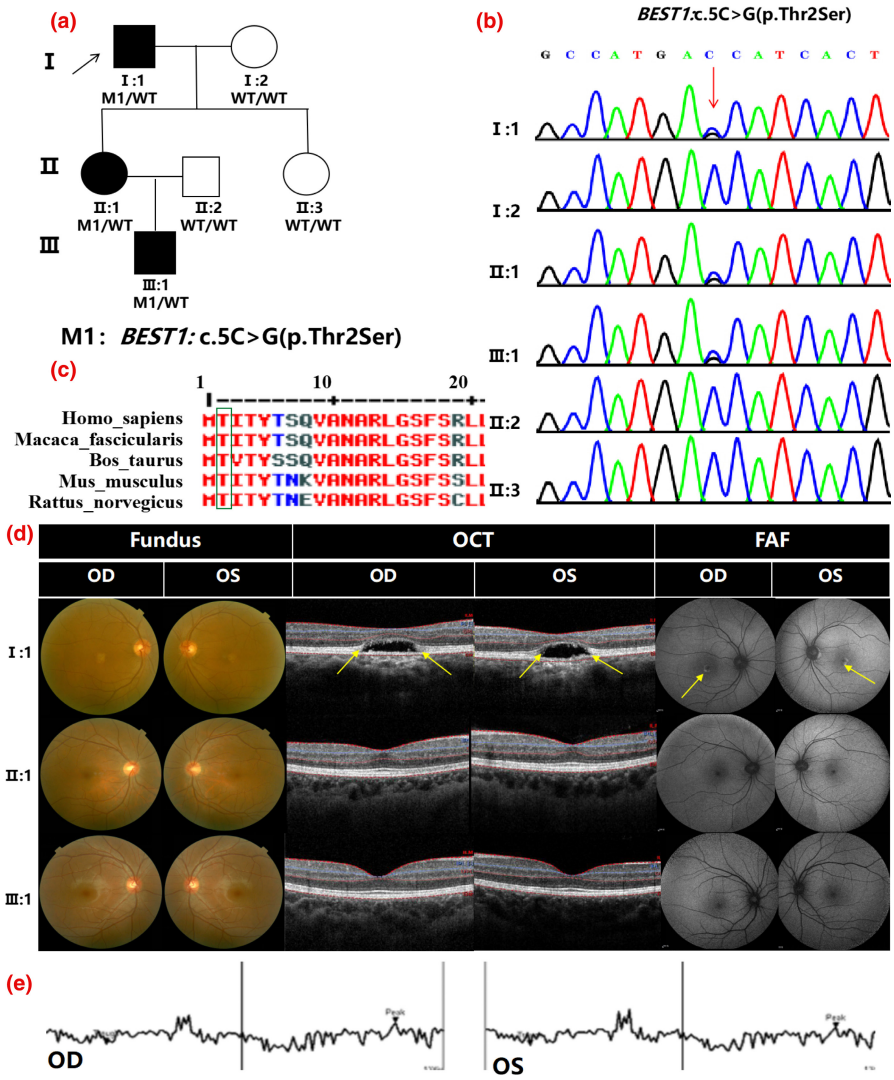

FIGURE 2 The pedigree, sequence analysis, and fundus examination of family 2 with AVMD. (a) Pedigree of family 2; (b) Sequence chromatograms of identified mutations; (c) The homology of amino acid sequences between human *BEST1* and other species. The amino acid at position 2 is highly conserved among species. The mutated residue 2 is boxed and indicated; (d) Fundus photograph: The proband (I:1) had a fried-egg-like appearance in the macula of both eyes, and no obvious abnormal changes were found in the macula of the other patients; OCT: In the proband (I:1), the macular fovea disappeared in both eyes, the ellipsoid zone was arched, the continuity of chimeric zone was interrupted, and the serous detachment of retinal nerve sensory layer. The structures of each layer of the daughter (II:1) and grandson (III:1) of the proband were complete and continuous without obvious abnormalities; FAF: The proband (I:1) can see uneven high fluorescence surrounding the macular fovea of both eyes, and other patients were normal. (e) The proband's EOG: the waveforms of dark valleys and light peaks are shown from left to right

by fundus photography and minor lesions could be detected by OCT in two patients. All of them had abnormal EOG (expect II:4) and one with abnormal FAF. The clinical data of ocular examination are shown in Table 1 and Figure 1.

A new heterozygous variant c.88A > G (p.Lys30Glu) was detected in the *BEST1* gene of the proband (Figure 1a,b), and its pathogenicity was clear according to ACMG guidelines. Her mother, brother, sister, and son all carried the same variant, suggesting co-segregation of genotype and clinical phenotype. Combined with the genotype and clinical phenotype, the patient was diagnosed with Best vitelliform macular dystrophy (BVMD) at the vitelliform stage. The other four heterozygous variant carriers in the family were determined as BVMD at previtelliform stage.

3.1.2 | Family 2

The proband, male, 67 years old, complained of blurred vision and visual distortion in the right eye for 2 weeks. He denied any inherited disease of family history. He had a normal color vision and BCVA of 0. 15 in the right eye, and 0.5 in the left eye. There was a small (about 1/2 DD

TABLE 2 Results of electrooculogram in three families with autosomal dominant Bestrophinopathies

Object		Right eye			Left eye		
		Dark through (μV)	Light peak (μV)	Arden ratio	Dark through (μV)	Light peak (μV)	Arden ratio
F1 patient	II:1 (29 y)	409.2	878.9	2.1	404.8	477.5	1.2
	I:2 (51 y)	640.6	873.0	1.4	796.9	1000.0	1.3
	II:3 (28 y)	262.7	520.5	2.0	398.4	813.0	2.0
	III:1 (7 y)	571.7	813.4	1.4	542.0	845.7	1.6
F1 normal	II:2 (32 y)	1200.0	2500.0	2.2	1100.0	2200.0	2.1
F2 patient	I:1 (67 y)	284.2	604.5	2.1	259.3	529.3	2.0
	II:1 (41 y)	544.4	868.2	1.6	441.9	705.6	1.6
	III:1 (12 y)	169.9	604.5	3.6	204.6	499.0	2.4
F3 patient	II:2 (16 y)	241.2	597.2	2.5	319.3	525.9	1.7
	I:2 (45 y)	417.0	805.2	1.9	574.7	879.9	1.5

Note: In the three autosomal dominant Bestrophinopathies families, the amplitudes of light peak potential and dark through potential decreased significantly in all patients, and the Q value (Arden ratio) of most patients was normal due to both the decrease of the amplitudes of light peak potential and dark through potential. It is worth noting that the rising value (peak) of EOG was very low under bright lighting.

in size), well-demarcated, fried-egg-like macular change in both eyes and no obvious abnormalities in the optic disc, peripheral retina, and blood vessels (Figure 2). The EOG was abnormal (Table 2), and full-field ERG was normal. His eldest daughter and grandson had no visible signs of the disease by fundus photography and OCT examination in both eyes, except for abnormal EOG. The clinical data of ocular examination are shown in Table 1 and Figure 2.

A known *BEST1* heterozygous variant c.5C>G (p.Thr2Ser) was detected on the proband (Figure 2a,b), and its pathogenicity is clear. His eldest daughter and grandson all carried the same variant, suggesting co-segregation of genotype and clinical phenotype. Combined with the genotype and clinical phenotype, the proband was diagnosed as adult-onset vitelliform macular dystrophy (AVMD) and classified as vitelliruptive stage. The other two heterozygous variant carriers in the family were diagnosed as AVMD at the previtelliform stage.

3.1.3 | Family 3

The proband, male, 16 years old, complained of vision loss in the right eye for 6 months. He denied any inherited disease of family history. He had a normal color vision and BCVA of 0.5 on the right eye and 1.0 on the left eye. There are some subretinal fibrosis and pigment precipitates in the macular and numerous very fine deposits anterior to the temporal vascular arcades in both eyes, and choroidal neovascularization in the macula of the right eye. He had abnormal EOG and normal full-field ERG (Table 2). The BCVA in the right eye was up to 1.0 one month after the anti-VEGF injection. His mother carried the same variant with BCVA 0.6 in the right eye and 1.0 in the left eye and classic vitelliform lesions centered on the fovea of both eyes. Also, EOG was abnormal. The clinical data of ocular examination are shown in Table 1 and Figure 3.

Heterozygous missense variant c.898G>A (p.Glu300Lys) was detected on the *BEST1* gene in the proband and his mother (Figure 3a,b) and its pathogenicity is clear. The genotype and clinical phenotype were co-segregated in this family. Combined with the genotype and clinical phenotype, the patient was diagnosed with Best vitelliform macular dystrophy (BVMD) at the atrophy and cicatricial stage, and his mother was confirmed as BVMD at the vitelliform stage.

3.1.4 | Family 4

The proband, female, 47 years old, was visited due to "decreased vision" and had previously been diagnosed with glaucoma. She denied any inherited disease of family history. BCVA was 0.1 on the right eye, 0.02 on the left eye, and intraocular pressure (IOP) was normal in both eyes (Table 3). The Iris laser holes can be seen in both eyes, and the anterior segment and vitreous body are normal. There was a "scrambled-egg" appearance of the macular lesion and extramacular scattered punctate deposits in both eyes (Figure 4 F4). EOG was abnormal (Table 4) and full-field ERG showed a severe decrease in scotopic 0.01 ERG, a moderate decrease in scotopic 3.0 ERG, and a mild reduction of photopic 3.0 ERG in both eyes.

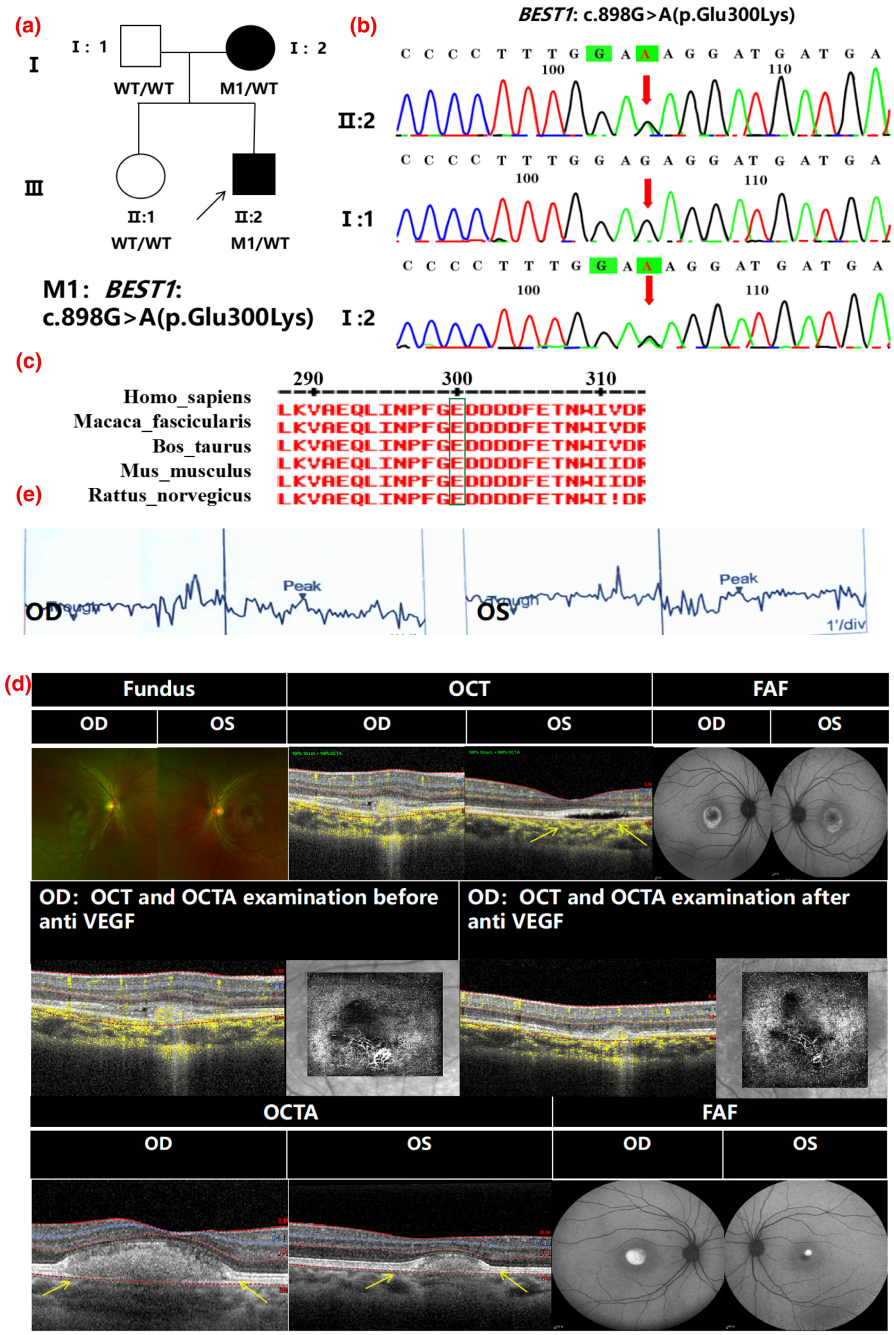

FIGURE 3 The pedigree, sequence analysis and fundus examination of family 3 with BVMD. (a) Pedigree of family 3; (b) Sequence chromatograms of identified mutations; (c) The homology of amino acid sequences between human *BEST1* and other species. The amino acid at position 300 is highly conserved among species. The mutated residue 300 is boxed and indicated; (d) Fundus photograph: The proband (II:2) had scattered yolk-like substance deposition in the macular area of both eyes, atrophy of retina and choroid, depigmentation, and accumulation; OCT: The macular fovea disappeared in the right eye, the chimeric zone and RPE band were broken, hyperreflective masses were visible below the chimeric zone, the continuity of ellipsoid zone and chimeric zone in the macular region of the left eye was interrupted, and the retinal nerve sensory layer was serous detachment; FAF: The yolk like substance in the macula area of both eyes of the proband shows circular high fluorescence and low fluorescence in the center; OCTA: Before anti-VEGF, the morphology and shape of deep retinal vascular plexus in the right eye were irregular, the knitted reticular structure was incomplete, the arch ring was deformed, and rough irregular abnormal vascular reticular structure could be seen. One month after anti-VEGF, the abnormal vascular reticular structure was reduced by OCT examination; The mother of the proband (I:2) OCT: The macular fovea of both eyes are raised, the ellipsoid zone and the chimeric zone are arched, and hyperreflective masses can be seen below the chimeric zone; FAF: The yolk like lesions in the macular area of both eyes showed high fluorescence. (e) The proband's EOG: the waveforms of dark valleys and light peaks are shown from left to right

TABLE 3 Clinical phenotypes of probands in three ARB families

Object	Best-corrected visual acuity		Fundus	Optical coherence tomography	FFA/FAF	Electrooculogram
	OD	OS				
F4 II:1 (47 y)	−0.50 DC × 50* = 0.1	PL = 0.02	"Scrambled-egg" and extramacular scattered punctate deposits	OD:the structures of chimeric zone, ellipsoid zone, and external membrane are disordered; Several shallow serous detachments of RPE, OS:interruption of RPE continuity and several hyperreflective masses.	FFA:low fluorescence, and the atrophic area of RPE shows plaque like high fluorescence.	Abnormal
F5 II:1 (12 y)	PL = 1.0	PL = 0.8	Yellow spotty and plaque-like precipitates	Serous detachment of the retinal neurosensory layer in both eyes, hyperreflective material was visible between the RPE/Bruch complex zone and interdigitation zone in the left eye.	FAF:a macular vertically elliptical hyperfluorescent ring with centered a low fluorescence region with scattered dots with high fluorescence in the left eye.	Abnormal
F6 II:2 (37 y)	PL = 1.0 → 0.8 → 0.4 → CF	PL = 1.0 → 0.6 → 0.4 → CF	Circular, well-circumscribed, yellow-opaque, less vitelliform contents macular lesion in both eyes	The detachment of retinal neuroepithelial layers and subretinal fluid accumulation.	FAF: low fluorescence in the macular area of both eyes, surrounded by high fluorescence.	Abnormal

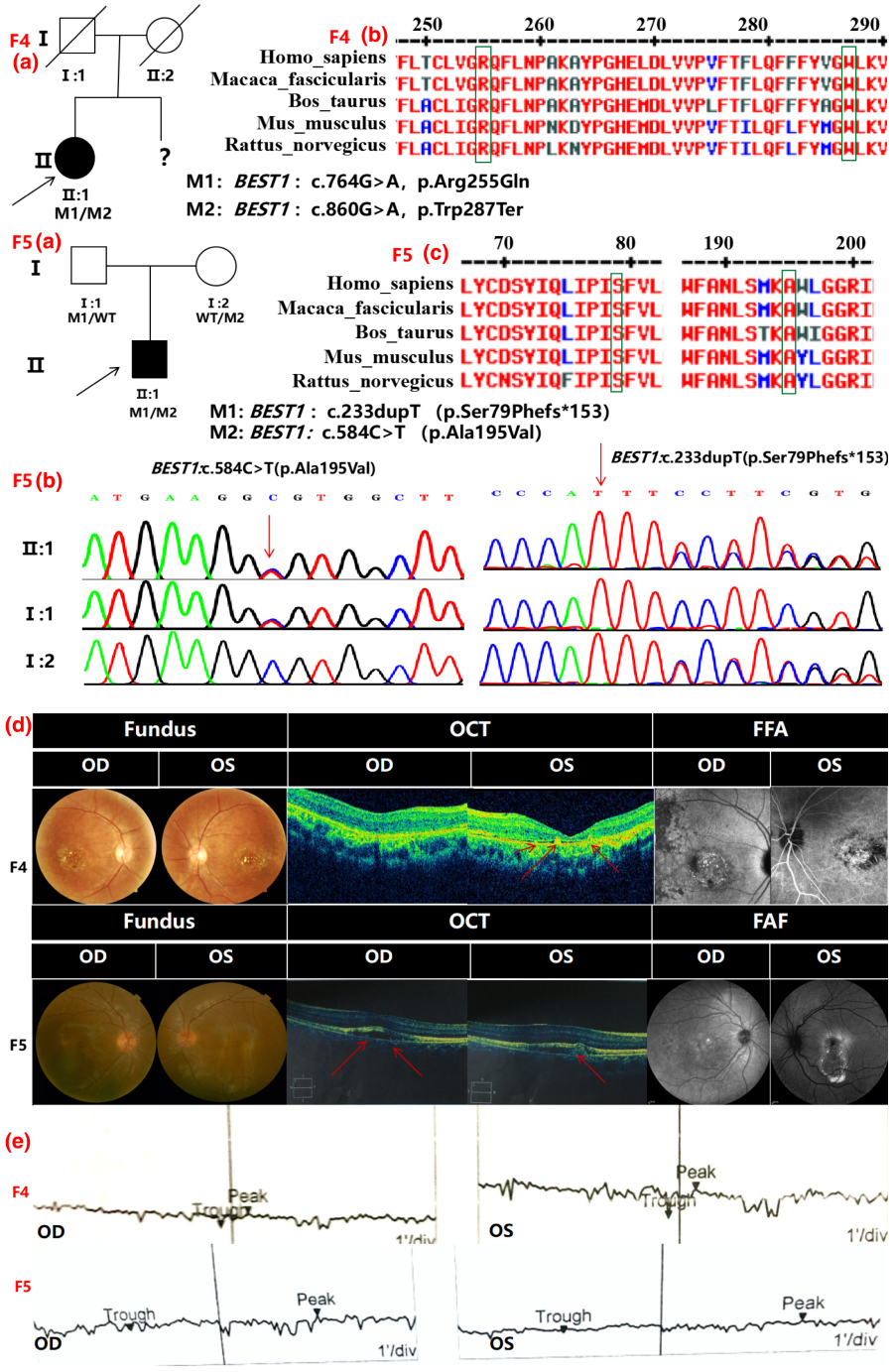

FIGURE 4 The pedigree, sequence analysis, and fundus examination of family 4 and family 5 with ARB. (F4a, F5a) Pedigrees of Family 4 and Family 5; (F4b) The homology of amino acid sequences between human BEST1 and other species. The amino acid at positions 255 and 287 are highly conserved among species. The mutated residue 255 and 287 are boxed and indicated; (F5b) Sequence chromatograms of identified mutations; (F5c) The homology of amino acid sequences between human BEST1 and other species. The amino acids at positions 195 and 79 were highly conserved among species. Mutated residues 195 and 79 are boxed and indicated; (d) Fundus photograph: In F4 proband, the "scrambled-egg" appearance of the macular lesion and extramacular scattered punctate deposits of both eyes can be seen. OCT: The macular fovea of the right eye is elevated, and the structures of the chimeric zone, ellipsoid zone, and external membrane are disordered; Several shallow serous detachments of retinal neuroepithelial layer, interruption of RPE continuity, and several hyperreflective masses can be seen in the left eye. FFA: The focus area of both eyes is low fluorescence, and the atrophic area of retinal pigment epithelium shows plaque-likee high fluorescence. Fundus photograph: In the F5 proband, yellow spotty and plaque-like precipitates were visible for the proband in the macula of both eyes. OCT showed serous detachment of the retinal neurosensory layer in both eyes, in which hyperreflective material was visible between the RPE/Bruch complex zone and interdigitation zone in the left eye. FAF revealed a macular vertically elliptical hyperfluorescent ring centered in a low fluorescence region with scattered dots with high fluorescence in the left eye. (e) The proband's EOG of F4 and F5:the waveforms of dark valleys and light peaks are shown from left to right

TABLE 4 Electrooculogram results of three ARB probands

Object	Right eye			Left eye		
	Dark through (μV)	Light peak (μV)	Arden ratio	Dark through (μV)	Light peak (μV)	Arden ratio
F4 II:1 (47 y)	142.6	316.4	2.2	200.2	559.1	2.8
F5 II:1 (12 y)	317.4	462.9	1.5	136.2	215.3	1.6
F6 II:2 (37 y)	368.2	515.6	1.4	405.3	605.0	1.5

The compound heterozygous variants c.764G > A (p.Arg255Gln) and c.860G > A (p.Trp287Ter) were detected on the *BEST1* gene of the proband (Figure 4 F4a, F4b), a missense variant and a nonsense variant, respectively, and its pathogenicity is clear. The parents of the proband were deceased, and the genetic origin was unclear. But the proband could be diagnosed as ARB according to the genetic test results and clinical phenotype.

3.1.5 | Family 5

The proband, male, 12 years old, came for a routine ophthalmologic examination. He denied any inherited disease of family history. BCVA was 1.0 on the right eye and 0.8 on the left eye. IOP, anterior segment, and vitreous were normal in both eyes (Table 3). The yellow spotty and plaque-like precipitates in the macula were visible in both eyes of the proband. OCT showed serous detachment of the retinal neurosensory layer in both eyes, in which hyperreflective material was visible between the RPE/Bruch complex zone and interdigitation zone in the left eye (Figure 4 F5). EOG was abnormal (Table 4), full-field ERG: The dark response 0.01 ERG b-wave amplitude was mildly decreased in both eyes, the dark adaptation 3.0 ERG b-wave amplitude was average, and the light adaptation 3.0 ERG b-wave amplitude was moderately reduced.

The compound heterozygous variants c.233dupT (p.Ser79Phefs*153) and c.584C > T (p.Ala195Val) were detected on the *BEST1* gene of the proband (Figure 4 F5a, F5b), a frameshift variant (from the mother) and a missense variant (from the father), respectively, and its pathogenicity is clear. And the parents were phenotypically normal, suggesting co-segregation of genotype and clinical phenotype.

It was consistent with autosomal recessive inheritance and was diagnosed as an ARB by combining the genotype and clinical phenotype of the patient.

3.1.6 | Family 6

The proband, male, 37 years old, presented to our hospital with "vision loss in both eyes for two years." He denied family history. Binocular vision was 0.4, IOP, anterior segment, and vitreous were normal (Table 3). Circular, well-circumscribed, yellow-opaque, less vitelliform contents macular lesion in both eyes, and OCT showed the detachment of retinal neuroepithelial layers and subretinal fluid accumulation. (Figure 5). EOG was abnormal (Table 4), full-field ERG: There was a mild decrease in dark response 0.01 ERG b-wave amplitude in both eyes, a mild decrease in dark adaptation 3.0 ERG b-wave amplitude, a moderate decrease in a-wave amplitude, and a mild decrease in light adaptation 3.0 ERG b-wave amplitude. This patient was diagnosed with CSC and given symptomatic treatment 2 years ago (September 2014). At that time, the BCVA was up to 1.0, the fundus photography was unknown, and the OCT results were as described above. After reexamination 6 months later (March 2015), the BCVA of the right eye was 0.8 and the BCVA of the left eye was 0.6, and the detachment of retinal neuroepithelial layers and subretinal fluid accumulation was not improved. Then FFA was performed and the diagnosis was corrected as binocular macular degeneration. After two anti-VEGF injections in the same year, the detachment of retinal neuroepithelial layers and subretinal fluid accumulation still existed. The visual acuity did not improve and tended to decrease gradually. The patient was followed up until March 2021, and his visual acuity was reduced to finger count in both eyes.

The compound heterozygous variants c.1070C > T (p.Ala357Val) (derived from the father) and c.427G > T (p.Val143Phe) (derived from the mother), both missense variants, were detected on the *BEST1* gene in the proband (Figure 5-1a), and its pathogenicity is clear. As validated by Sanger, it presented co-segregation of the genotype and clinical phenotype. It was consistent with autosomal recessive inheritance and was diagnosed as ARB by combining the genotype and clinical phenotype of the patient.

3.2 | Pathogenicity analysis of identified variants (bioinformatics analysis)

Nine different variants were detected in six pedigrees, three of which are not yet included in HGMD and are considered as novel variants.

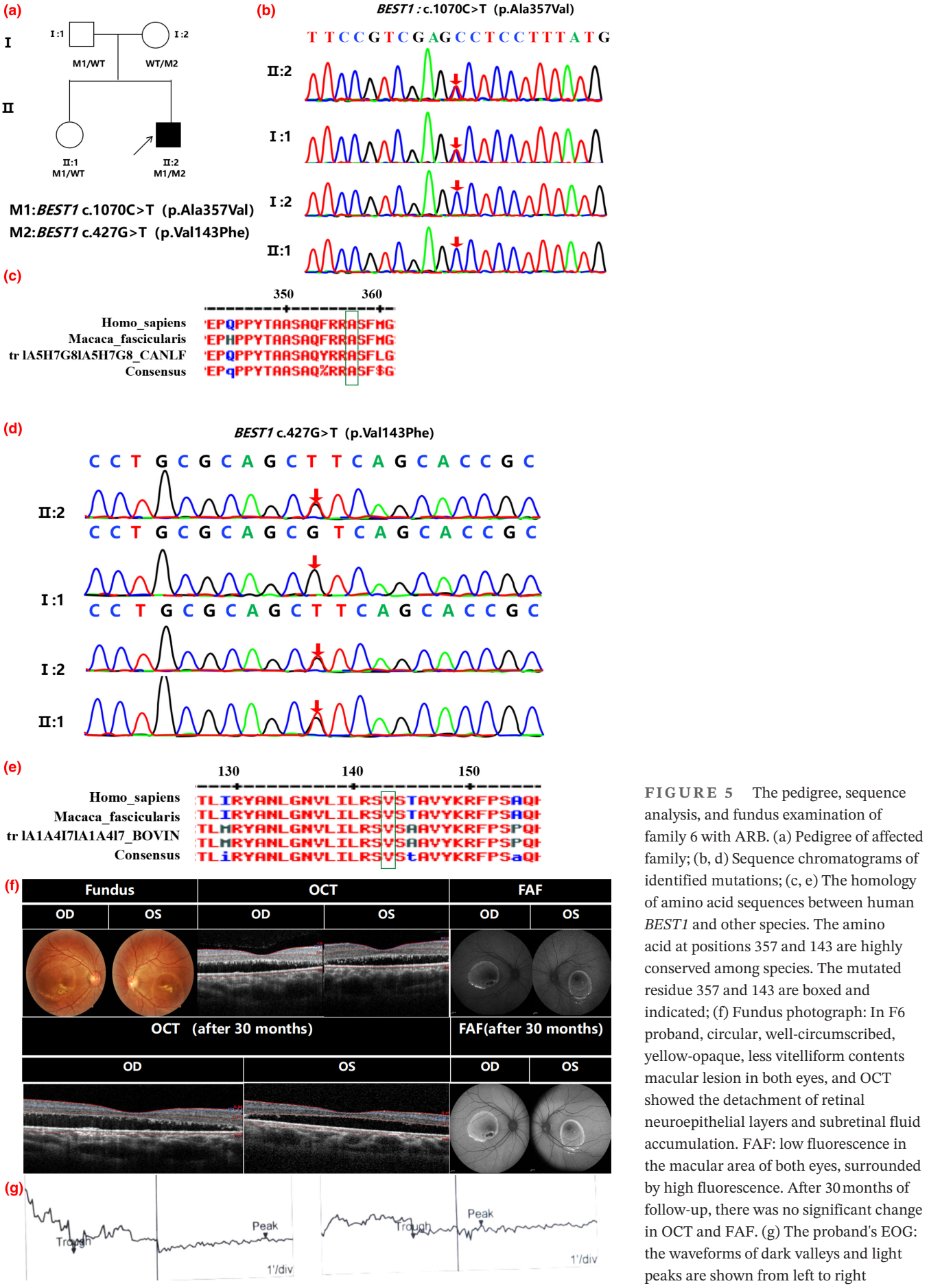

FIGURE 5 The pedigree, sequence analysis, and fundus examination of family 6 with ARB. (a) Pedigree of affected family; (b, d) Sequence chromatograms of identified mutations; (c, e) The homology of amino acid sequences between human *BEST1* and other species. The amino acid at positions 357 and 143 are highly conserved among species. The mutated residue 357 and 143 are boxed and indicated; (f) Fundus photograph: In F6 proband, circular, well-circumscribed, yellow-opaque, less vitelliform contents macular lesion in both eyes, and OCT showed the detachment of retinal neuroepithelial layers and subretinal fluid accumulation. FAF: low fluorescence in the macular area of both eyes, surrounded by high fluorescence. After 30 months of follow-up, there was no significant change in OCT and FAF. (g) The proband's EOG: the waveforms of dark valleys and light peaks are shown from left to right

3.2.1 | Autosomal dominant variant in *BEST1*

A novel missense variant c.88A > G (p.Lys30Glu) (PM5_Supporting) was initially detected in exon 2 of the *BEST1* gene in the Family 1 proband (II:1) by exome, and show segregation in the family (PP1_Supporting). The search for the Genome Aggregation Database (gnomAD) and the East Asian Population Database (ExAC EAS) showed that the variant frequency of this variant was equal to 0 (PM2_Supporting). What is more, the amino acid at position 30 was highly conserved among different species by proteomic conservation analysis (Figure 1c), indicating that the variant at this site is more likely to affect the structure and function of *BEST1* protein (PP3_Supporting).

Heterozygous missense variant c.5C > G (p.Thr2Ser) and c.898G > A (p.Glu300Lys) were detected in Family 2 proband (I:1) and Family 3 proband (II:2) by exome, respectively. Then segregated the disease status, these variants were later confirmed in all affected members by Sanger sequencing (PP1_Supporting). These variants were previously reported in the pieces of literature that such variant has been detected in patients with BVMD and the relevant information has been included in the HGMD and the Clinvar database (PS1_Strong) (Gao et al., 2020; Guo et al., 2019; Liu et al., 2016). These substitutions, c.5C > G and c.898G > A, would cause the amino acid change, four software kits suggested the deleterious impact of this substitution and indicated that the variant at these sites is more likely to affect the structure and function of *BEST1* protein (PP3_Supporting). What is more, the amino acids at positions 2 and 300 were highly conserved among different species by proteomic conservation analysis (Figures 2 and 3c), indicating that these variants are more likely to affect the structure and function of *BEST1* protein (PP3_Supporting).

3.2.2 | Autosomal recessive variant in *BEST1*

The compound heterozygous variants c.764G > A (p.Arg255Gln) and c.860G > A (p.Trp287Ter) were detected on the Family 4 proband (II:1). The former has not been previously reported and the mutation frequency in the East Asian Population Database (ExAC_EAS) was very low (PM2_Supporting). The latter is known to be associated with Bestrophinopathies and the relevant information is included in the HGMD and the Clinvar database (PS1_Strong) (MacDonald et al., 2012; Tian et al., 2017). The substitution, c.764G > A, would cause the amino acid change from Arginine to Glutamine at residue 255 (p.Arg255Gln), and four software kits suggested the deleterious impact of this substitution. The nonsense variant, c.860G > A, was predicted to generate a premature termination codon at residue 287, which would result in premature termination of polypeptide chain synthesis, and most of the proteins produced were inactive or lost their normal function (PVS1_Very Strong). What is more, the amino acids at position 255 and 287 were highly conserved among different species by proteomic conservation analysis (Figure 4 F4b), indicating that the two variants at these sites are more likely to affect the structure and function of *BEST1* protein (PP3_Supporting).

The compound heterozygous variants c.233dupT (p.Ser79Phefs*153) and c.584C > T (p.Ala195Val) were detected in Family 5 proband (II:2), which segregated the disease status (PP1_Supporting). The frameshift variant has not been previously reported and was also not detected in the East Asian Population Database (ExAC_EAS) (PM2_Supporting). The c.233dupT variant causes a frameshift starting with codon Serine79, changes this amino acid to a Phenylalanine residue, and creates a premature Stop codon at position 153 of the new reading frame, denoted p.Ser79Phefs*153 (PP3_supporting). This frameshift variant was located in the loss-of-function region (LOF) and affected the protein function (PVS1_Very Strong). The substitution, c.584C > T, would cause the amino acid change from Alanine to Valine at residue 195 (p.Ala195Val), which was previously reported in several patients with Bestrophinopathies and the relevant information has been included in the HGMD and the Clinvar database (PS1_Strong) (Davidson et al., 2011; Gerth et al., 2009). Four software kits suggested the deleterious impact of this substitution (PP3_supporting).

The compound heterozygous variants c.1070C > T (Ala357Val) and c.427G > T (p.Val143Phe) were detected in Family 6 proband (II:2), which segregated the disease status (Figure 5b,d) (PP1_Supporting). The former variant would cause the amino acid change from Alanine to Valine at residue 357 (p.Ala357Val), and four software suggested the deleterious impact of this substitution (PP3_supporting). The latter substitution, c.427G > T, would cause the amino acid change from Valine to Phenylalanine at residue 143 (p.Val 143Phe) and it has been reported in the HGMD database to be associated with Adult vitelliform macular dystrophy (PS1_Strong) (Kinnick et al., 2011). Four software kits suggested the deleterious impact of this substitution. What is more, the amino acid at positions 357 and 143 was highly conserved among different species by proteomic conservation analysis (Figure 5c,e), indicating that the two variants at these sites are more likely to affect the structure and function of *BEST1* protein (PP3_Supporting).

To sum up, each of the nine pathogenic variants is most likely the causative variant for the disease phenotype in the corresponding family (Table 5). This is because:

TABLE 5 Pathogenic mutations and prediction of *BEST1 of* nine variations *in* six probands with Bestrophinopathies

No.	Chromosome[a]	Exon	Nucleotiide change	Amino acid change	Gene	Mutation types	Status	Novel or known	Disease	Prediction			Allele frequency	
										Polyphen-2 (HVAR/HDIV)	SIFT	PROVEAN	Mutation taster	ExAC	GnomAD
F1	chr11:61719366	2	c.88A>G	p.Lys30Glu	*BEST1*	Missense	Het	Novel	BVMD	0.999/0.999 (D)	0.001 (D)	−3.66 (D)	0.999 (D)	–	–
F2	chr11:61719283	2	c.5C>G	p.Thr2Ser	*BEST1*	Missense	Het	Known	AVMD	0.998/0.998 (D)	0.000 (D)	−3.64 (D)	0.999 (D)	–	0.000007
F3	chr11:61727000	8	c.898G>A	p.Glu300Lys	*BEST1*	Missense	Het	Known	BVMD	0.952/0.952 (D)	0.001 (D)	−3.38 (D)	0.999 (D)	–	–
F4	chr11:61725667	7	c.764G>A	p.Arg255Gln	*BEST1*	Missense	Het	Novel	ARB	1.000/1.000 (D)	0.116 (T)	−3.90 (D)	0.999 (D)	0.000016	0.000007
	chr11:61725763	7	c.860G>A	p.Trp287Ter	*BEST1*	Nonsense	Het	Known		–	–	–	1.000 (D)	0.000017	0.000012
F5	chr11:61722658	3	c.233dupT	p.Ser79 Phefs*153	*BEST1*	Frameshift	Het	Novel	ARB	–	–	–	1.000 (D)	–	–
	chr11:61724418	5	c.584C>T	p.Ala195Val	*BEST1*	Missense	Het	Known		0.388/0.388 (B)	0.001 (D)	−3.71 (D)	0.999 (D)	0.000247	0.000157
F6	chr11:61727485	9	c.1070C>T	p.Ala357Val	*BEST1*	Missense	Het	Known	ARB	0.026/0.026 (B)	0.027 (D)	−1.19 (N)	0.947 (P)	0.00163	0.000385
	chr11:61723369	4	c.427G>T	p.Val143Phe	*BEST1*	Missense	Het	Known		0.920/0.092 (D)	0.001 (D)	−4.70 (D)	0.999 (D)	–	–

[a]NC_000011.9:61717293–61,732,987, Homo sapiens, chromosome 11, GRCh37.p13.

(1) Three novel variants were observed in the database of normal subjects of the sequencing company with a very low variant frequency. (2) Six known variants have been reported in the HGMD database to be associated with Bestrophinopathies. (3) There are no other potential pathogenic variants detected in this study. (4) The well-established correlations between the genes mutated and the disease phenotypes for each family.

4 | DISCUSSION

Bestrophinopathies are emerging as the second most common macular lesion, affecting approximately 1 in 10,000 (Rahman et al., 2019). *BEST1* is mainly expressed on the RPE and is associated with the onset of a series of fundus diseases such as BVMD, AVMD, ARB, ADVIRC, retinitis pigmentosa-50 (RP-50, OMIM 613914), microcornea, rod-cone dystrophy, cataract, and posterior staphyloma syndrome, potentially affecting the development of entire eyeball, especially the anterior segment abnormalities, such as the shallow anterior chamber, narrow angle of anterior chamber, short axial-length, and microphthalmia (Boon et al., 2009; Smith et al., 2019). Most of the *BEST1* gene variants are missense variants, and a few are splice site variants and synonymous variants, with most mutant sites clustered in the N and C termini and four transmembrane regions within the cell (Boon et al., 2013). A total of 9 variants were reported in this paper, 3 of which were novel and contained a total of 77.8% (7/9) missense variants, 11.1% (1/9) nonsense variants, and 11.1% (1/9) frameshift variants. For autosomal dominant Bestrophinopathies, the variants in Family 1 (exon2) and Family 3 (exon8) were located in known hotspot regions, such as four amino acid regions 6–30, 80–104, 221–243, and 293–312 of exon2, 4, 6, and 8 (Boon et al., 2009). In contrast, the variant in family 2 (exon 2) was not in the hot spot region. For autosomal recessive Bestrophinopathies, the variants are mostly concentrated in exons 5 and 7 (Gao et al., 2020), and in this paper, the variants in the ARB probands were also distributed in exons 3, 4, and 9 except for exons 5 and 7, which were the transmembrane region or topological domain. Recently, an increasing number of studies have shown that the variant spectrum is different between different ethnic groups (Gao et al., 2020; Tian et al., 2017). For example, p.R255W may be a common recessive variant in Asian patients (Luo et al., 2019; Tian et al., 2017). Common mutant loci reported in other races were not seen in the nine variants identified in this paper. In addition, *BEST1* and *PRPH2* were reported in the literature as the two major genes associated with the AVMD phenotype (Grunin et al., 2016; Tiosano et al., 2016). Some scholars believe that AVMD is a manifestation of BVMD

in adult-onset, and some reports confirm that patients with AVMD conform to an autosomal dominant mode of inheritance and have an overlapping portion of the phenotype with BVMD. The data of this study are consistent with it. The genotype and phenotype of Family 2 in this paper suggest that AVMD is predominantly inherited in an AD manner and overlaps with the phenotype of BVMD, which is consistent with the high degree of genetic heterogeneity in genotype and phenotype due to variants in the *BEST1* gene.

Interestingly, the phenotype of autosomal dominant Bestrophinopathies is irregular dominant inheritance, in which some patients show a typical vitelliform lesion in the macular and the others show no visible signs of the disease in the family carrying the same pathogenicity heterozygous variant. It has been reported that the penetrance rate of Bestrophinopathies is 96%. The penetrance rate of 3 families (BVMD or AVMD) in this paper was as high as 100%, without forme frust (heterozygotes that are not expressed at all), but the expressivity of each heterozygote was variable. In Family 1, five affected individuals all carried the same heterozygous variant, but the severity of the macular lesions varied widely. Among them, the proband showed typical vitelliform lesions in the macula, while the other 5 patients had no visible signs of the disease by fundus photography and minor lesions could be detected on OCT in two patients. All of them (expect II:4) had abnormal EOG and one with abnormal FAF. Notably, the mother of the proband (I:2), 51 years old, had normal appearing fundi, and OCT showed minor macular structural abnormalities with disruption of the ellipsoid zone and interdigitation zone in the right eye. It also showed irregular dominance in family 2 and family 3. At the present time, the mechanism of this irregular dominant inheritance was unknown. The distinct intrafamilial phenotypic diversity might be due to enhanced/weakened action of the modifier gene on the primary gene so that the traits determined by the primary gene were not expressed or incompletely expressed and showed varying expressivities, or they might be due to the influence of the organism's internal and external environment. Even though the expressivity varies, heterozygous individuals with a dominant gene can still pass such traits to their offspring even if they do not exhibit the dominant trait themselves or to a lesser extent, which data highlight the need for extensive molecular evaluations in the family with an autosomal dominant variant in *BEST1*. Moreover, phenotypes due to autosomal recessive variants in the *BEST1* gene is also highly heterogeneous, ranging from vitelliform lesions to extensive extramacular deposits (peripheral flecks). The severity of the phenotype is related to the homozygote status. Homozygous variants result in a typical phenotype of ARB, while compound heterozygous variants result in atypical ARB resembling the BVMD phenotype or AVMD phenotype. Such clinical heterogeneity may be influenced by the external environment or may result from the interaction between different variants on the double alleles. The most common features of ARB are extramacular scattered punctate deposits and intraretinal and subretinal fluid (SRF) accumulation. In this study, the proband of family 4 showed a "scrambled-egg" appearance of macular lesion and extramacular scattered punctate deposits. OCT showed the detachment of retinal neuroepithelial layers and subretinal fluid accumulation in the left eye with disrupted RPE continuity. As described above, this proband not only had the phenotype recognizably resembling vitelliruptive stage of BVMD but also had some features of ARB, such as extramacular scattered punctate deposits. The proband of family 5 showed fairly normal fundi by ophthalmoscopy in both eyes, but FAF revealed a macular vertically elliptical hyperfluorescent ring with centered a low fluorescence region with scattered dot high fluorescence in the left eye, and OCT showed serous detachment of the retinal neurosensory layer in both eyes, the hyperreflective material was visible between the RPE/Bruch complex zone and interdigitation zone in the left eye. This proband had the phenotype recognizably resembling the pseudohypopyon phase of BVMD, such as FAF imaging in the left eye. In Family 6, the proband showed circular, well-circumscribed, yellow-opaque, less vitelliform contents macular lesion in both eyes, similar to the manifestation at the vitelliruptive stage of BVMD, OCT showed the detachment of retinal neuroepithelial layers and subretinal fluid accumulation. During the follow-up period of up to 30 months, the presence of subretinal fluid and vitelliform sediment did not change significantly with time. This is consistent with the report of Casalino et al. (2021).

The pathogenic mechanism of Bestrophinopathies is still unclear, so there is no effective treatment. For asymptomatic patients with an autosomal dominance variant in the *BEST1* gene, it can continue to be passed on in the family, leading to blindness in the next generation due to the heritability of the disease, which suggests that genetic testing and counseling are essential to be required. In ARB patients who are usually complicated by narrow angle of the anterior chamber, laser iridotomy can be performed as early as possible and the angle of the anterior chamber can be monitored regularly to avoid elevated intraocular pressure in closed-angle glaucoma, which can aggravate visual impairment, as in Family 4 proband in this study. Patients who are complicated with choroidal neovascularization (CNV) can be treated with anti-VEGF medication. The

visual acuity of Family 3 proband was recovered to 1.0 after anti-VEGF treatment for CNV in the right eye, and no significant decrease in visual acuity was seen after six months of follow-up, which is consistent with previous reports in the literature (Hussain et al., 2015). For ARB patients who are complicated with macular edema, oral administration of Methazolamide may help to reduce such macular edema; Panpan Ye et al. (2020) found a significant decrease in the levels of certain metabolites, such as citric acid, L-threonine, and eicosapentaenoic acid, in the blood of ARB patients and found significant improvement in macular edema after long-term supplementation of citric acid in these patients. In recent years, research on the treatment of Bestrophinopathies has yielded fruitful results and it will surely usher in a promising spring.

5 | SUMMARY

This study provided evidence that the phenotype of autosomal dominant bestrophinopathies (VMD) was part of irregular dominant inheritance due to reduced penetrance and variable expressivity, with patients carrying a pathogenic heterozygous variant of *BEST1* to develop obviously intrafamilial phenotypic diversity. The patients who harbor two heterozygous variants showed recessive inheritance bestrophinopathies with distinct phenotypic diversity ranging from typical/atypical vitelliform lesions to extensive extramacular deposits (peripheral flecks). Our study also emphasized the importance of comprehensive genetic analysis in patients with bestrophinopathies, and in such challenging families with markedly intrafamilial phenotypic diversity, it shall provide novel insights into phenotypic assessments of bestrophinopathies and contribute to better diagnosis, prognosis, and treatment for these patients. Further study on different pathogenic mechanisms of the *BEST1* gene variant may better explain its phenotypic diversity and will improve the diagnosis and treatment of these patients in the future.

AUTHOR CONTRIBUTIONS

The authors alone are responsible for the content and writing of the article. Zhen Li completed processing cases and data. Xunlun Sheng and Weining Rong revised and polished the article. Meijiao Ma and Rui Qi collected case data of Family 4 and Family 5, respectively. All authors read and approved the final manuscript.

ACKNOWLEDGMENTS

The authors thank all patients and their family members for their participation.

FUNDING INFORMATION

This work was supported by the National Natural Science Foundation of China (81760180), the Key R & D Plan Project of Ningxia Hui Autonomous Region (2021BEG02045), the key research and development project of Ningxia Hui Autonomous Region (2020BEG03047), the training project of the scientific innovation commanding talented person in Ningxia Hui Autonomous Region (KJT2020013) and Ningxia Natural Science Foundation Project (2021AAC03302).

CONFLICT OF INTEREST

The authors declare that they have no competing interests.

DATA AVAILABILITY STATEMENT

The datasets presented in this study can be found in online repositories. The names of the repository and accession number can be found below: Banklt repository (BankIt (https://www.ncbi.nlm.nih.gov/WebSub/) ID: 2639801, 2639805-2639809, 2639812, 2639813, 2639815).

CONSENT FOR PUBLICATION

Not applicable.

ETHICS APPROVAL AND CONSENT TO PARTICIPATE

Our research complies with the declaration of Helsinki and has been approved and reviewed by the human research ethics committee of the people's Hospital of Ningxia Hui Autonomous Region. Each participant or their legal guardian signed the informed consent form.

ORCID

Shangying Yang https://orcid.org/0000-0001-8970-7501

REFERENCES

Boon, C. J., Klevering, B. J., Leroy, B. P., Hoyng, C. B., Keunen, J. E., & den Hollander, A. I. (2009). The spectrum of ocular phenotypes caused by mutations in the BEST1 gene. *Progress in Retinal and Eye Research*, *28*(3), 187–205. https://doi.org/10.1016/j.preteyeres.2009.04.002

Boon, C. J., van den Born, L. I., Visser, L., Keunen, J. E., Bergen, A. A., Booij, J. C., Riemslag, F. C., Florijn, R. J., & van Schooneveld, M. J. (2013). Autosomal recessive bestrophinopathy: Differential diagnosis and treatment options. *Ophthalmology*, *120*(4), 809–820. https://doi.org/10.1016/j.ophtha.2012.09.057

Casalino, G., Khan, K. N., Armengol, M., Wright, G., Pontikos, N., Georgiou, M., Webster, A. R., Robson, A. G., Grewal, P. S., & Michaelides, M. (2021). Autosomal recessive Bestrophinopathy: Clinical features, natural history, and genetic findings in preparation for clinical trials. *Ophthalmology*, *128*(5), 706–718. https://doi.org/10.1016/j.ophtha.2020.10.006

Chowers, I., Tiosano, L., Audo, I., Grunin, M., & Boon, C. J. (2015). Adult-onset foveomacular vitelliform dystrophy: A fresh perspective. *Progress in Retinal and Eye Research*, *47*, 64–85. https://doi.org/10.1016/j.preteyeres.2015.02.001

Davidson, A. E., Millar, I. D., Burgess-Mullan, R., Maher, G. J., Urquhart, J. E., Brown, P. D., Black, G. C. M., & Manson, F. D. C. (2011). Functional characterization of bestrophin-1 missense mutations associated with autosomal recessive bestrophinopathy. *Investigative Ophthalmology & Visual Science*, *52*(6), 3730–3736. Published 2011 Jun 1. https://doi.org/10.1167/iovs.10-6707

Gao, F. J., Qi, Y. H., Hu, F. Y., Wang, D. D., Xu, P., Guo, J. L., Li, J. K., Zhang, Y. J., Li, W., Chen, F., Xu, G. Z., Liu, W., Chang, Q., & Wu, J. H. (2020). Mutation spectrum of the bestrophin-1 gene in a large Chinese cohort with bestrophinopathy. *The British Journal of Ophthalmology*, *104*(6), 846–851. https://doi.org/10.1136/bjophthalmol-2019-314679

Gerth, C., Zawadzki, R. J., Werner, J. S., & Héon, E. (2009). Detailed analysis of retinal function and morphology in a patient with autosomal recessive bestrophinopathy (ARB). *Documenta Ophthalmologica*, *118*(3), 239–246. https://doi.org/10.1007/s10633-008-9154-5

Grunin, M., Tiosano, L., Jaouni, T., Averbukh, E., Sharon, D., & Chowers, I. (2016). Evaluation of the association of single nucleotide polymorphisms in the PRPH2 gene with adult-onset foveomacular vitelliform dystrophy. *Ophthalmic Genetics*, *37*(3), 285–289. https://doi.org/10.3109/13816810.2015.1059456

Guo, J., Gao, F., Tang, W., Qi, Y., Xuan, Y., Liu, W., Li, L., Ye, X., Xu, G., Wu, J., & Zhang, Y. (2019). Novel BEST1 mutations detected by next-generation sequencing IN a CHINESE POPULATION with vitelliform macular dystrophy. *Retina*, *39*(8), 1613–1622. https://doi.org/10.1097/IAE.0000000000002183

Hussain, R. N., Shahid, F. L., Empeslidis, T., & Ch'ng, S. W. (2015). Use of intravitreal bevacizumab in a 9-year-old child with choroidal neovascularization associated with autosomal recessive Bestrophinopathy. *Ophthalmic Genetics*, *36*(3), 265–269. https://doi.org/10.3109/13816810.2014.962706

Jay, W. M. (2012). Genetic diseases of the eye. *Neuro-Ophthalmology*, *36*(4), 174.

Johnson, A. A., Guziewicz, K. E., Lee, C. J., Kalathur, R. C., Pulido, J. S., Marmorstein, L. Y., & Marmorstein, A. D. (2017). Bestrophin 1 and retinal disease. *Progress in Retinal & Eye Research*, *58*, 45–69. https://doi.org/10.1016/j.preteyeres.2017.01.006

Kinnick, T. R., Mullins, R. F., Dev, S., Leys, M., Mackey, D. A., Kay, C. N., Lam, B. L., Fishman, G. A., Traboulsi, E., Iezzi, R., & Stone, E. M. (2011). Autosomal recessive vitelliform macular dystrophy in a large cohort of vitelliform macular dystrophy patients. *Retina*, *31*(3), 581–595. https://doi.org/10.1097/IAE.0b013e318203ee60

Liu, J., Zhang, Y., Xuan, Y., Liu, W., & Wang, M. (2016). Novel BEST1 mutations and special clinical features of BEST vitelliform macular dystrophy. *Ophthalmic Research*, *56*(4), 178–185. https://doi.org/10.1159/000444681

Luo, J., Lin, M., Guo, X., Xiao, X., Li, J., Hu, H., Xiao, H., Xu, X., Zhong, Y., Long, S., Luo, G., Mi, L., Chen, X., Fang, L., Wei, W., Zhang, Q., & Liu, X. (2019). Novel BEST1 mutations and special clinical characteristics of autosomal recessive bestrophinopathy in Chinese patients. *Acta Ophthalmologica*, *97*(3), 247–259. https://doi.org/10.1111/aos.13994

MacDonald, I. M., Gudiseva, H. V., Villanueva, A., Greve, M., Caruso, R., & Ayyagari, R. (2012). Phenotype and genotype of patients with autosomal recessive bestrophinopathy. *Ophthalmic Genetics*, *33*(3), 123–129. https://doi.org/10.3109/13816810.2011.592172. Epub 2011 Aug 2. PMID: 21809908.

Marmorstein, A. D., Johnson, A. A., Bachman, L. A., Andrews-Pfannkoch, C., Knudsen, T., Gilles, B. J., Hill, M., Gandhi, J. K., Marmorstein, L. Y., & Pulido, J. S. (2018). Mutant Best1 expression and impaired phagocytosis in an iPSC model of autosomal recessive Bestrophinopathy. *Scientific Reports*, *8*(1), 4487.

Mullins, R. F., Oh, K. T., Heffron, E., Hageman, G. S., & Stone, E. M. (2005). Late development of vitelliform lesions and flecks in a patient with Bestrophinopathies: Clinicopathologic correlation. *Archives of Ophthalmology*, *123*(11), 1588–1594. https://doi.org/10.1001/archopht.123.11.1588

Rahman, N., Georgiou, M., Khan, K. N., & Michaelides, M. (2019). Macular dystrophies: Clinical and imaging features, molecular genetics and therapeutic options. *British Journal of Ophthalmology*, *104*(4), 451–460. https://doi.org/10.1136/bjophthalmol-2019-315086

Richards, S., Aziz, N., Bale, S., Bick, D., das, S., Gastier-Foster, J., Grody, W. W., Hegde, M., Lyon, E., Spector, E., Voelkerding, K., Rehm, H. L., & ACMG Laboratory Quality Assurance Committee. (2015). Standards and guidelines for the interpretation of sequence variants: A joint consensus recommendation of the American College of Medical Genetics and Genomics and the Association for Molecular Pathology. *Genetics in Medicine*, *17*(5), 405–424. https://doi.org/10.1038/gim.2015.30

Smith, J. J., Nommiste, B., & Carr, A. F. (2019). Bestrophin1: A gene that causes many diseases. *Advances in Experimental Medicine and Biology*, *1185*, 419–423. https://doi.org/10.1007/978-3-030-27378-1_69

Soria, R. B., Spitzner, M., Schreiber, R., & Kunzelmann, K. (2009). Bestrophin-1 enables Ca2+−activated Cl- conductance in epithelia. *Journal of Biological Chemistry*, *284*(43), 29405–29412.

Tian, L., Sun, T., Xu, K., Zhang, X., Peng, X., & Li, Y. (2017). Screening of BEST1 gene in a Chinese cohort with BEST vitelliform macular dystrophy or autosomal recessive Bestrophinopathy. *Investigative Ophthalmology & Visual Science*, *58*(9), 3366–3375. https://doi.org/10.1167/iovs.17-21999

Tiosano, L., Grunin, M., Hagbi-Levi, S., Banin, E., Averbukh, E., & Chowers, I. (2016). Characterising the phenotype and progression of sporadic adult-onset foveomacular vitelliform dystrophy. *The British Journal of Ophthalmology*, *100*(11), 1476–1481. https://doi.org/10.1136/bjophthalmol-2015-307658

Tsang Stephen, H., & Tarun, S. (2018). Best vitelliform macular dystrophy. *Advances in Experimental Medicine and Biology*, *1085*, 79–90.

Vincent, A., Mcalister, C., Vandenhoven, C., & Heon, E. (2011). BEST1-related autosomal dominant vitreoretinochoroidopathy: A degenerative disease with a range of developmental ocular anomalies. *Eye*, *25*(1), 113–118.

Wood, S. R., McClements, M. E., Martinez-Fernandez de la Camara, C., Patrício, M. I., Uggenti, C., Sekaran, S., Barnard, A. R., Manson, F. D., & MacLaren, R. E. (2019). A Quantitative Chloride Channel Conductance Assay for Efficacy Testing of AAV.BEST1. *Human Gene Therapy Methods*, *30*(2), 44–52.

Ye, P., Xu, J., Luo, Y., Su, Z., & Yao, K. (2020). Familial autosomal recessive bestrophinopathy: Identification of a novel variant in BEST1 gene and the specific metabolomic profile. *BMC Medical Genetics*, *21*(1), 16. Published 2020 Jan 22. https://doi.org/10.1186/s12881-020-0951-3

How to cite this article: Yang, S., Li, Z., Cheng, W., Ma, M., Qi, R., Rui, X., Ren, Y., Sheng, X., & Rong, W. (2023). *BEST1* novel mutation causes Bestrophinopathies in six families with distinct phenotypic diversity. *Molecular Genetics & Genomic Medicine*, *11*, e2095. https://doi.org/10.1002/mgg3.2095